Petroleum Science (2018) 15:882–889
https://doi.org/10.1007/s12182-018-0267-5

ORIGINAL PAPER

Polyoxometalate-based silica-supported ionic liquids for heterogeneous oxidative desulfurization in fuels

Ming Zhang[1] · Miao Wang[1,2] · Jiapeng Yang[2] · Hongping Li[1] · Jiaqi Liu[1,2] · Xiao Chen[3] · Wenshuai Zhu[3] · Huaming Li[1]

Received: 14 April 2018 / Published online: 10 October 2018

Abstract
With the aim of deep desulfurization, silica-supported polyoxometalate-based ionic liquids were successfully prepared by a one-pot hydrothermal process and employed in heterogeneous oxidative desulfurization of various sulfur compounds. The compositions and structures of the hybrid samples were characterized by various methods such as FT-IR, XPS, Raman, UV–Vis, wide-angle XRD and N_2 adsorption–desorption. The experimental results indicated that the hybrid materials presented a high dispersion of tungsten species and excellent catalytic activity for the removal of 4,6-dimethyldibenzothiophene without any organic solvent as extractant, and the sulfur removal could reach 100.0% under mild conditions. The catalytic performance on various substrates was also investigated in detail. After cycling seven cycles, the sulfur removal of the heterogeneous system still reached 93.0%. The GC-MS analysis results demonstrated that the sulfur compound was first adsorbed by the catalyst and subsequently oxidized to its corresponding sulfone.

Keywords Polyoxometalate · Silica-supported ionic liquid · Heterogeneous oxidative desulfurization

1 Introduction

In the past years, new energy sources such as solar power and hydrogen energy in the auto industry have been springing up. However, fuel oil still occupies a dominant position. Sulfur compounds in fuel oil generate sulfur oxides (SO_x) after combustion, and this is a main source of acid rain, haze and other environmental issues (Zhang et al. 2017a; Ibrahim et al. 2017). Thus, most countries have implemented strict standards to limit the sulfur content in fuel oil to below 10 ppm. Up to now, conventional hydrodesulfurization (HDS) is efficient in removing thiols, sulfides and disulfides, but not efficient for the removal of heterocyclic sulfur compounds such as dibenzothiophene and its derivatives, especially 4,6-dimethyldibenzothiophene (Zhang et al. 2017b; Li et al. 2016). Accordingly, the development of alternative desulfurization progress is in the ascendant, including biodesulfurization (Soleimani et al. 2007), adsorption desulfurization (Ren et al. 2018; Yang et al. 2018), extraction desulfurization (Rafiee et al. 2016) and oxidative desulfurization (Akopyan et al. 2015; Zhang et al. 2014). Among these, oxidative desulfurization is considered to be the most promising technology due to its mild operating conditions and high removal efficiency for the heterocyclic sulfur compounds mentioned above (Zhang et al. 2013).

Ionic liquids (ILs) with unique physicochemical properties have been widely employed as solvents, extractants, templates and precursors (Zhou and Qu 2017; Dai et al. 2017). In the desulfurization process, ionic liquids are often used as extractants (Paduszyński et al. 2017; Moghadam et al. 2017), but the sulfur removal is not so satisfactory. Thus, polyoxometalates (POMs), a family of transition

Edited by Xiu-Qin Zhu

Handling editor: Wenshuai Zhu

✉ Wenshuai Zhu
zhuws@ujs.edu.cn

✉ Huaming Li
lhm@ujs.edu.cn

[1] Institute for Energy Research, Jiangsu University, Zhenjiang 212013, China

[2] School of Energy and Power Engineering, Jiangsu University, Zhenjiang 212013, China

[3] School of Chemistry and Chemical Engineering, Jiangsu University, Zhenjiang 212013, China

metal–oxide clusters with specific physical properties and controllable redox and properties, are often introduced as anions to the family of specific ILs (Zhao et al. 2012; Zhu et al. 2013). In the oxidative desulfurization, POM-based ILs could not only capture the sulfur compounds from oil but also activate the oxidant (e.g., hydrogen peroxide) to oxidize the sulfur compounds to sulfones. The desulfurization performance of POM-based ILs was desirable, but the catalytic systems often suffered from some problems such as high dosage and low specific area of ILs, difficulty in the separation of catalyst (Xun et al. 2016; Li et al. 2015). Thus, immobilization of POM-based ILs on a suitable carrier (e.g., silica) is a good method to solve the above problems.

Hence, in this work, a series of molybdenum-containing silica-supported ionic liquids $[C_4mim]_3PMo_{12}O_{40}/SiO_2$ were designed to achieve the advantages of both the POM materials and heterogeneous catalysis. The hybrid materials $[C_4mim]_3PMo_{12}O_{40}/SiO_2$ from a one-pot hydrothermal method were highly efficient in the oxidative desulfurization of 4,6-dimethyldibenzothiophene and other sulfur compounds, where no organic solvents were added as extractants. Moreover, the samples were also systematically characterized by XRD, XPS, FT-Raman, FT-IR, UV–Vis and N_2 adsorption–desorption analysis.

2 Experimental section

2.1 Chemicals and materials

n-octane (CP grade), $H_3PMo_{12}O_{40}\cdot 26H_2O$ (AR grade), acetonitrile (CH_3CN, AR grade), tetraethylorthosilicate (TEOS, AR grade), hydrogen peroxide (H_2O_2, 30 wt%) and ammonia ($NH_3\cdot H_2O$, 25 wt%) were acquired from Sinopharm Chemical Reagent Co. Ltd., China. Benzothiophene (BT, 99%), dibenzothiophene (DBT, 98%), 4-methyldibenzothiophene (4-MDBT, 98%) and 4,6-dimethyldibenzothiophene(4,6-DMDBT, 99%) were purchased from Sigma-Aldrich. $[C_4mim]Cl$ (99%) was obtained from Shanghai Chenjie Chemical Co. Ltd., China. All the reagents were used directly as received.

2.2 Synthesis of the catalysts

The ionic liquid $[C_4mim]_3PMo_{12}O_{40}$ was synthesized according to a previous study (Rajkumar and Rao 2008). Then, silica-supported ionic liquid was synthesized by a one-pot hydrothermal method as follows: Firstly, 0.17 g of $[C_4mim]_3PMo_{12}O_{40}$ was dissolved in 4 mL of acetonitrile at 50 °C under continuous stirring. After that, the solution above was added dropwise to 26 mL of deionized water under continuous stirring for 10 min and followed by addition of 2 mL of TEOS. Afterward, 0.5 mL of 25% aqueous ammonia was added to the mixture. After stirring for 3 h at room temperature, the mixture was transferred into the reactor and kept at 120 °C for 24 h. Then, the resultant was filtered and washed with deionized water three times and treated at 150 °C for 3 h. For comparison, other materials with different Mo:Si molar ratios and different treating temperatures were prepared by a similar method and denoted as x-$[C_4mim]_3PMo/SiO_2$-y (x = 0.05, 0.1 and 0.2, and y = 150, 200 and 250 °C).

2.3 Characterization

FT-IR spectra of the catalysts were recorded on a Nicolet Nexus 470 spectrometer using KBr pellets (Thermo Electron Corporation, USA). SEM imaging was performed on a JEOL JEM-7001F field-emission microscope (JEOL Corporation, Japan). XPS was collected on a PHI 530 with a monochromatic Mg Kα source (Ulvac-Phi Corporation, Japan). Raman spectroscopy was studied on a DXR Raman microscope (Thermo Fisher Scientific, USA) with a 532-nm excitation laser power. UV–visible spectra were recorded on a UV–Vis spectrometer (UV-2450, Shimadzu, Japan). X-ray diffraction patterns were recorded with a Bruker D8 diffractometer using Cu Kα radiation (λ = 1.5418 Å). The N_2 absorption–desorption isotherms were collected on a TriStar II 3020 surface area and porosity analyzer (Micromeritics Corporation, USA). The oxidation products of 4,6-DMDBT were studied by GC–MS on an Agilent 7890A (Agilent, USA).

2.4 Catalytic activity test

Model oil was obtained by dissolving the desired amount of BT, DBT, 4-MDBT and 4,6-DMDBT in *n*-octane to achieve a corresponding S-content of 250 ppm. A mixture of 0.01 g catalyst and 5 mL model oil was added into a two-necked reactor equipped with a magnetic stirrer and a condenser. Afterward, oxidation of sulfur compounds was carried out by adding a desired amount of H_2O_2 to the mixture above. After the reaction, the residual sulfur content was measured on GC-FID HP-5 MS column, 30 m×320 μm i.d.×0.25 μm; FID: Agilent, rising from 100 to 160 °C at a heating rate of 20 °C/min and then rising to 230 °C at a heating rate of 25 °C/min. The sulfur removal (%) was calculated as follows:

$$\text{Sulfur removal}\ (\%) = \frac{\text{Initial sulfur content} - \text{Residual sulfur content}}{\text{Initial sulfur content}} \times 100\%$$

3 Results and discussion

3.1 Characterization of samples

Figure 1 shows the FT-IR spectra of supported $[C_4mim]_3$PMo and IL. For $[C_4mim]_3$PMo (Fig. 1a), the peaks around 3145 and 3107 cm^{-1} belong to the stretching vibration of C–H of the alkyl chain. The peaks around 1564 and 1465 cm^{-1} are ascribed to the stretching vibration of C=N and scissoring vibration of C–H, respectively (Xun et al. 2014). In addition, the four characteristic absorption peaks of the Keggin structure of ionic liquid can be clearly observed in the range of 1100 to 750 cm^{-1}, belonging to ν_{as} (P–O_a), ν_{as} (Mo–O_t), ν_{as} (Mo–O_b–Mo) and ν_{as} (Mo–O_c–Mo), respectively (Dong et al. 2014). For IL supported on silica, the characteristic absorption peaks of the silica support were found around 3430 and 963 cm^{-1} caused by the stretching vibration of Si–OH on the silica surface, and the characteristic peaks at 1085, 807 and 470 cm^{-1} were attributed to the bending vibration of ν_{as} (Si–O–Si), ν_{as} (Si–O–Si) and silicate ions, respectively. The absorption bands for the POM anion could not be detected, as they were overlapped by the characteristic absorption of silica.

Further structural information about the various samples was obtained from Raman scattering spectroscopy (Fig. 2). For $[C_4mim]_3$PMo, the characteristic absorption peaks located at 1005 and 997 cm^{-1} could be clearly detected. These were ascribed to the vibration of ν_s (Mo–O_t) and ν_{as} (Mo–O_t), respectively. The bands ranging from 920 to 860 cm^{-1} and from 620 to 580 cm^{-1} could be ascribed to the vibration of ν_s (Mo–O_b–Mo) and ν_s (Mo–O_c–Mo), respectively. In addition, an strong absorption peak around 247 cm^{-1} was caused by the vibration of ν_s (Mo–O_a) (Sainero et al. 2001). For the IL-supported materials (Fig. 2b–f), as the IL contents increased from 0.05 to 0.2, the intensity of the characteristic absorption peaks around 1000 cm^{-1} also increased gradually. Other characteristic absorption peaks of the Keggin structure could also be found, indicating that the IL was successfully introduced. On the other hand, for silica-supported IL with different treatment temperatures, no peak shift was observed, indicating that the original structure of the ionic liquid did not change.

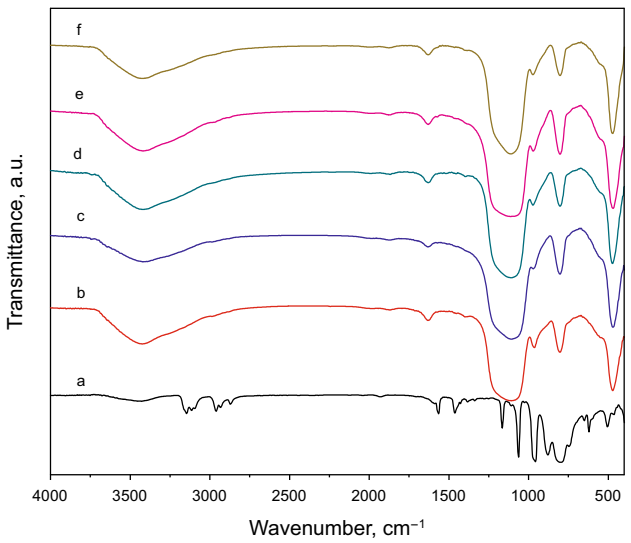

Fig. 1 FT-IR spectra of various samples: a $[C_4mim]_3$PMo, b 0.2$[C_4mim]_3$PMo/SiO_2-250, c 0.1$[C_4mim]_3$PMo/SiO_2-250, d 0.05$[C_4mim]_3$PMo/SiO_2-250, e 0.1$[C_4mim]_3$PMo/SiO_2-200 and f 0.1$[C_4mim]_3$PMo/SiO_2-150

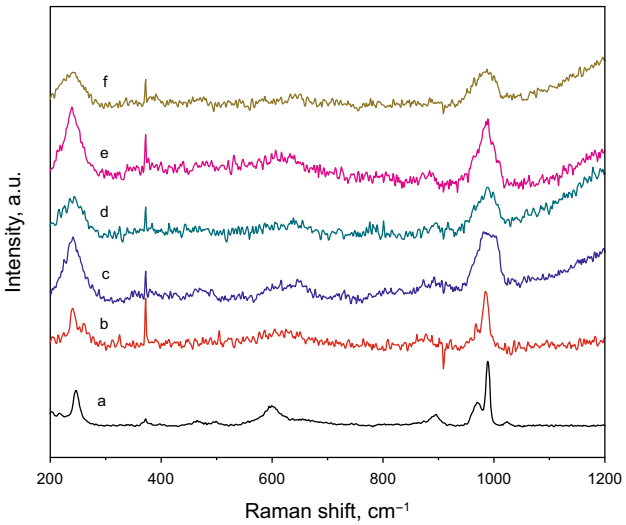

Fig. 2 Raman spectra of various samples: a $[C_4mim]_3$PMo, b 0.2$[C_4mim]_3$PMo/SiO_2-250, c 0.1$[C_4mim]_3$PMo/SiO_2-250, d 0.05$[C_4mim]_3$PMo/SiO_2-250, e 0.1$[C_4mim]_3$PMo/SiO_2-200 and f 0.1$[C_4mim]_3$PMo/SiO_2-150

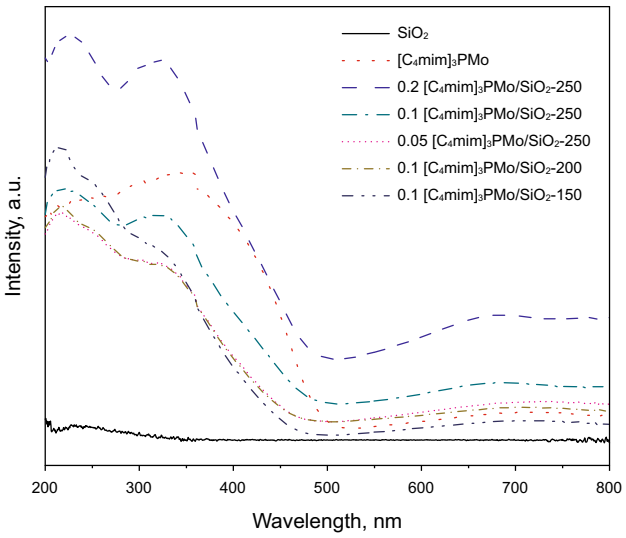

Fig. 3 UV-vis spectra of various materials

Figure 3 shows the electron transfer properties of various samples by UV–visible spectroscopy. For the supported silica, no obvious absorption was found. For $[C_4mim]_3PMo$, two absorption bands could be observed in the region of 220–320 nm, which were ascribed to the electron transfer from O–P and a ligand–metal charge transfer ($O^{2-} \rightarrow Mo^{6+}$), respectively (Liu et al. 2013). For the supported IL materials, it is observed that the intensity of the two characteristic absorption peaks mentioned changes clearly. As IL content increased, the intensity of characteristic absorption peaks in the UV–Vis range increased gradually.

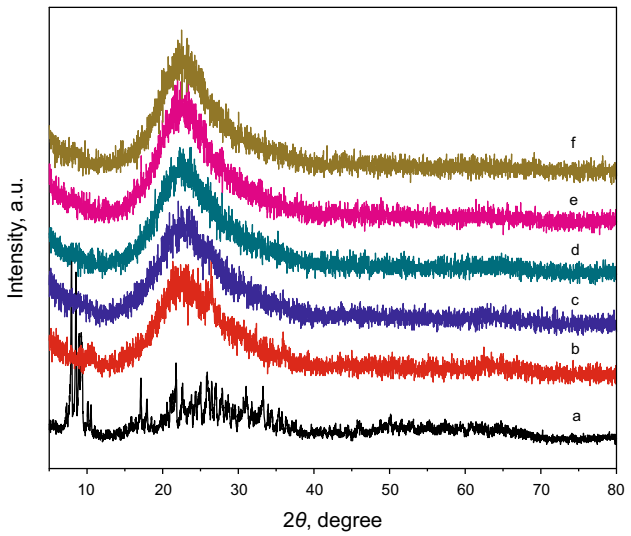

Fig. 4 XRD patterns of various materials: a $[C_4mim]_3PMo$, b 0.2 $[C_4mim]_3PMo/SiO_2$-250, c 0.1$[C_4mim]_3PMo/SiO_2$-250, d 0.05$[C_4mim]_3PMo/SiO_2$-250, e 0.1$[C_4mim]_3PMo/SiO_2$-200 and f 0.1$[C_4mim]_3PMo/SiO_2$-150

Figure 4 reveals the wide-angle XRD patterns of various materials. For $[C_4mim]_3PMo$, a series of sharp peaks can be detected in the 2θ range of 5°–35°. For supported IL materials with different IL contents, only a broad peak of amorphous silica could be observed instead of the diffraction of $[C_4mim]_3PMo$, which indicates a high dispersion of IL in the silica. However, for the sample 0.2$[C_4mim]_3PMo/SiO_2$-250, except for the amorphous peaks of amorphous silica, the diffraction peaks of $[C_4mim]_3PMo$ can be found around 26.5°, which could be ascribed to the aggregated IL with a high loading content.

To investigate the surrounding chemical environment and volatile valence of the active Mo atoms in the sample, XPS spectra were obtained (Fig. 5). As shown in Fig. 5a, the peaks located at 284.7, 398.8, 104.2, 134.5 and 233 eV are assigned to C 1s, N 1s, Si 2p, P 2p and Mo 3d respectively, indicating that $[C_4mim]_3PMo$ was successfully introduced. In addition, two distinct peaks belonging to Mo $3d_{5/2}$ and Mo $3d_{3/2}$ could be detected with binding energies of 232.7 and 236.2 eV, respectively, indicating the oxidation states of Mo^{6+} (Zhang et al. 2012). These results also demonstrated the ionic liquid maintained its original structure after introduction to silica.

Figure 6 shows N_2 absorption–desorption isotherms (Fig. 6a) and BJH pore size distribution curves (Fig. 6b) of various samples. In Fig. 6a, all the samples exhibited type IV with a clear H1-type hysteresis loop according to the IUPAC classification, indicating the presence of mesopores. Moreover, the hysteresis loop of the N_2 adsorption–desorption isotherm appears in the high relative pressure ($P_0/P > 0.8$), which was attributed to the accumulation of particles during the formation of the samples (Liu et al. 2012). The pore size distribution of the catalysts was measured by the BJH model. As shown in Fig. 6b, the pore

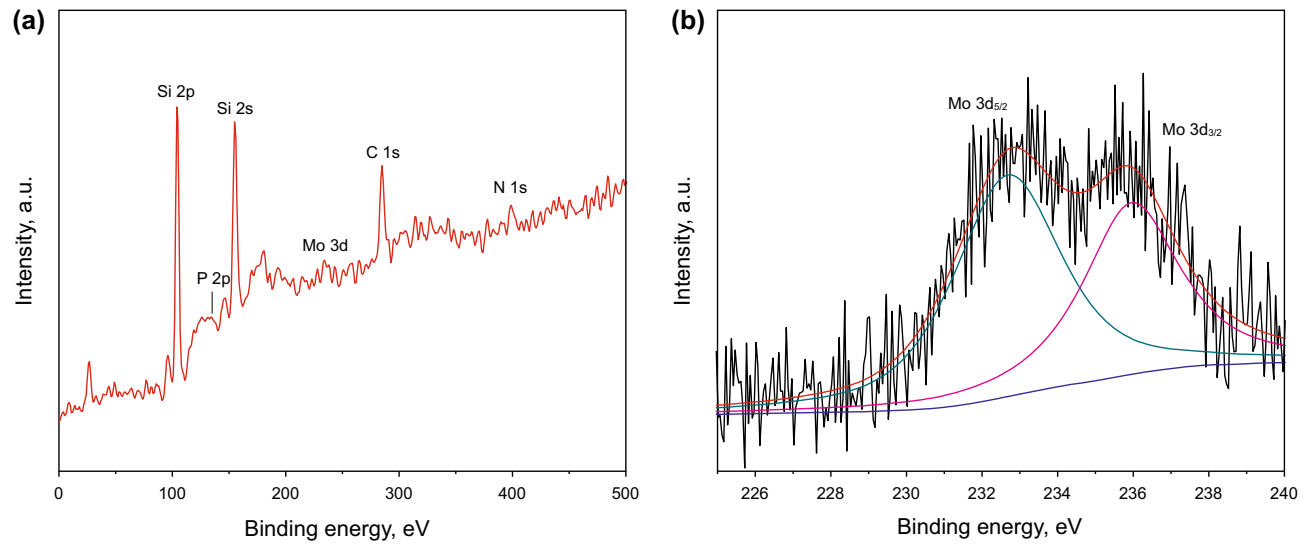

Fig. 5 XPS analysis survey (**a**) and Mo 3d core-level spectrum (**b**)

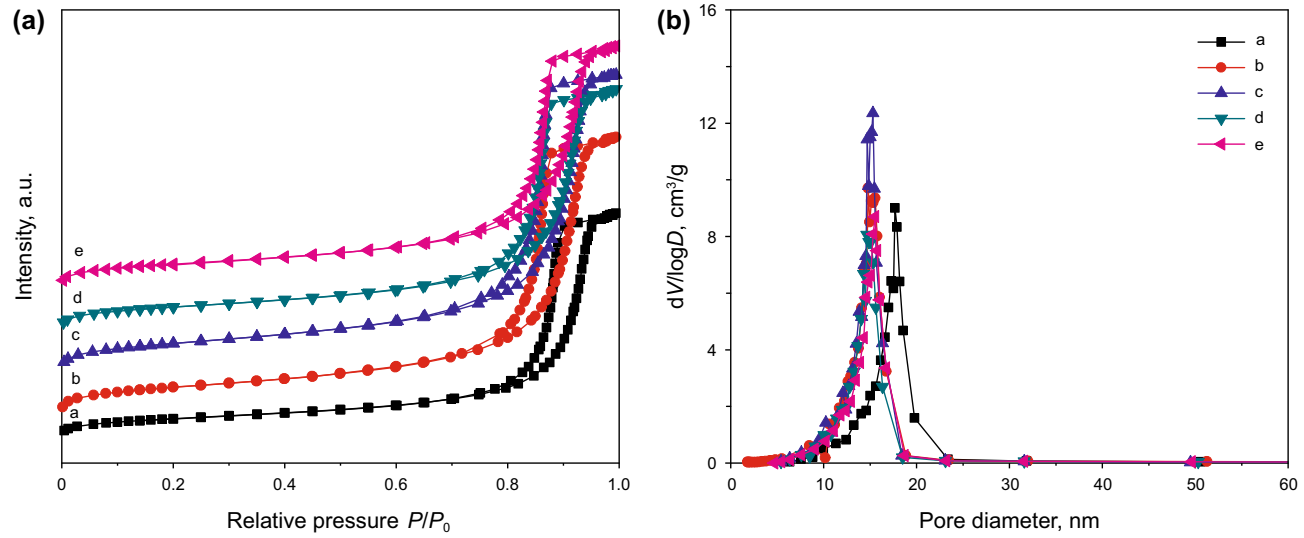

Fig. 6 N_2 adsorption–desorption isothermals (**a**) and BJH pore size distribution (**b**) of various materials: a 0.2[C_4mim]$_3$PMo/SiO_2-250, b 0.1[C_4mim]$_3$PMo/SiO_2-250, c 0.05[C_4mim]$_3$PMo/SiO_2-250, d 0.1[C_4mim]$_3$PMo/SiO_2-200 and e 0.1[C_4mim]$_3$PMo/SiO_2-150

Table 1 Structural properties of various samples

Entry	Samples	S_{BET}, $m^2\ g^{-1}$	Pore volume, $cm^3\ g^{-1}$
1	0.2[C_4mim]$_3$PMo/SiO_2-250	189.3	0.82
2	0.1[C_4mim]$_3$PMo/SiO_2-250	269.4	1.03
3	0.05[C_4mim]$_3$PMo/SiO_2-250	277.3	1.08
4	0.1[C_4mim]$_3$PMo/SiO_2-200	220.4	0.88
5	0.1[C_4mim]$_3$PMo/SiO_2-150	217.9	0.87

size distributions of all the samples are centered in the range of 10–20 nm. The specific surface areas and pore volumes of the samples are shown in Table 1. For the samples with the same treatment temperature (Entry 1–3, Table 1), the specific surface area and pore volume parameters decreased as the IL content increased. On the other hand, for the samples with different treatment temperatures (Entry 3–5, Table 1), the specific surface area increased from 217.9 to 277.3 $m^2\ g^{-1}$, and the pore volume increased from 0.87 to 1.03 $cm^3\ g^{-1}$, which may be caused by the compactness of the catalyst structure at higher temperature, leading to an increase of specific surface area and pore volume.

3.2 Catalytic performance

Figure 7 displays the performance of various samples on the removal of 4,6-DMDBT under the same conditions. For 0.1[C_4mim]$_3$PMo/SiO_2 with different treatment temperatures, it can be found that the catalytic performance increased with higher treatment temperature, which is ascribed to the increase of the specific surface area and pore volume, leading to the sufficient contact of the

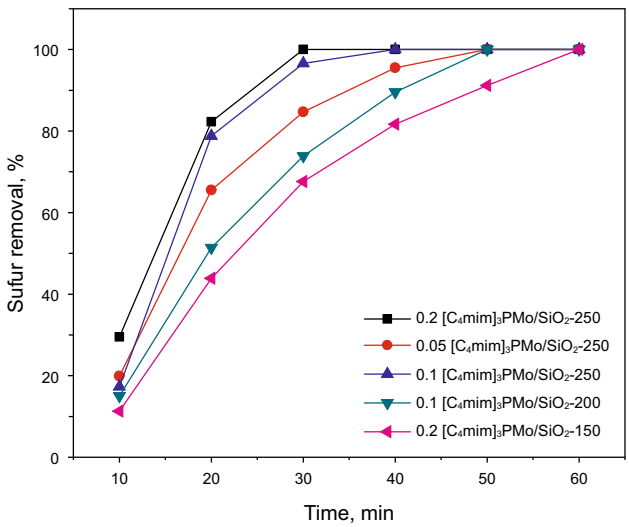

Fig. 7 Influence of various samples on the catalytic performance. Reaction conditions: mass of catalyst = 0.01 g, T = 60 °C, t = 60 min, molar ratio O/S = 3

catalyst active centers and the sulfur compounds. For [C_4mim]$_3$PMo/SiO_2-250 with different IL contents, it can be observed that the catalytic performance was improved

as the IL content increased. Although the increase of the IL content resulted in a decrease of the specific surface area and pore volume, the increase of active centers would also accelerate the reaction. The sulfur removal with the sample 0.1[C_4mim]$_3$PMo/SiO_2-250 could reach 100% in 40 min with an oxidant/sulfur molar ratio (O/S) =3.

Since real oil contains a variety of thiophene sulfides, the catalytic oxidation performance of various sulfur compounds including BT, DBT, 4-MDBT and 4,6-DMDBT is investigated using 0.1[C_4mim]$_3$PMo/SiO_2-250 as the typical catalyst in this study (Fig. 8). It is clearly observed that the desulfurization of various sulfur compounds decreased in the order of 4,6-DMDBT > 4-MDBT > DBT > BT. These results can be mainly accounted for by the different electron densities on the sulfur atom of 4,6-DMDBT, 4-MDBT, DBT and BT which were 5.760, 5.759, 5.758 and 5.739, respectively (Xu et al. 2009). 4,6-DMDBT has the largest electron density among the substrates, making it easy to be oxidized.

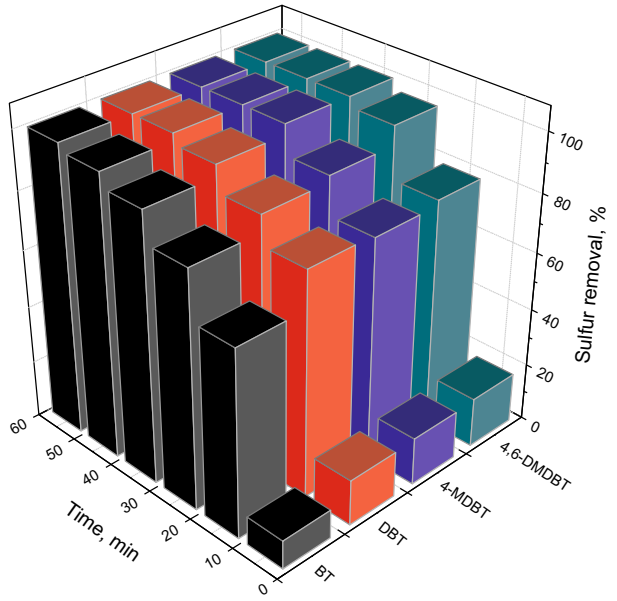

Fig. 8 Influence of various substrates on the catalytic performance. Reaction conditions: mass of catalyst = 0.01 g, T = 60 °C, t = 60 min, molar ratio O/S = 3

3.3 Analysis of oxidation product

To investigate the oxidation products of 4,6-DMDBT, GC-MS analysis was performed as shown in Fig. 9. After the reaction, the upper oil phase was directly decanted, and the lower catalyst was extracted by CCl_4 for GC-MS analysis. In Fig. 9a, it is observed that there is no peak for 4,6-DMDBT, and only an intense peak for *n*-tetradecane at 4.3 min could be detected. On the other hand (Fig. 9b), the peaks for 4,6-DMDBTO_2 (m/z = 244.1) and 4,6-DMDBT (m/z = 208.1) could be observed at 16.4 min and 9.9 min, respectively. These results demonstrated that 4,6-DMDBT was firstly adsorbed by the catalyst and subsequently oxidized to 4,6-DMDBTO_2.

3.4 Reusability of the catalyst

It is also important to investigate the recycling capability of the reaction system (Fig. 10). After the first reaction, the upper clear oil phase was directly decanted for separation, and the used catalyst (0.1[C_4mim]$_3$PMo/SiO_2-250) was dried at 50 °C overnight. Under the same conditions, fresh H_2O_2 and model oil were added for the next run. It is worth

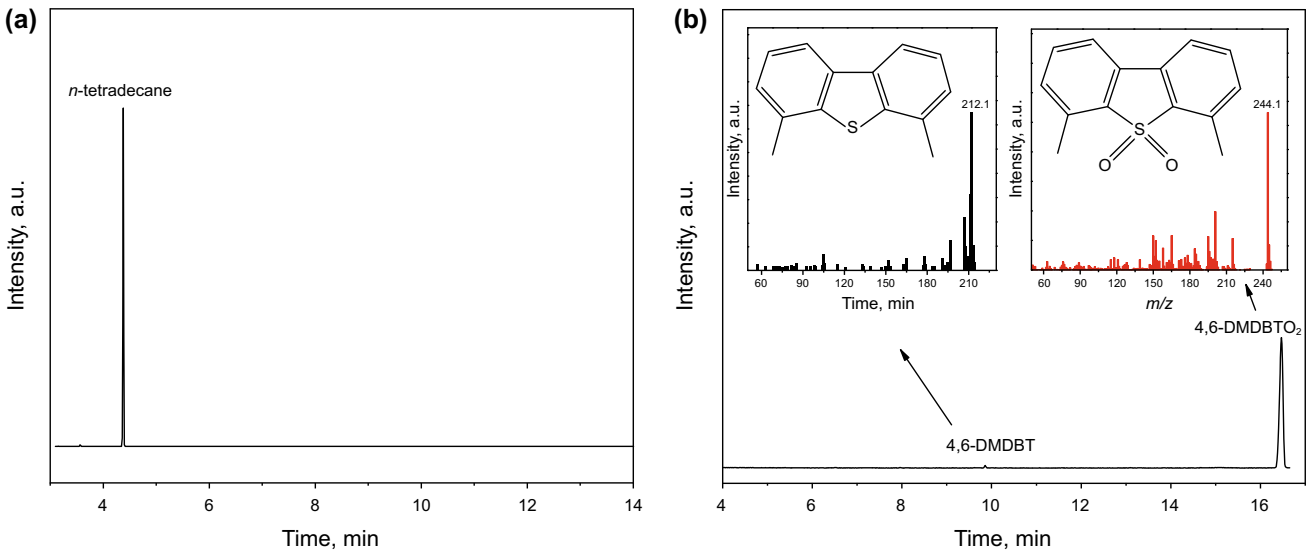

Fig. 9 GC-MS analysis of (**a**) upper oil phase after reaction and (**b**) extracted phase from the catalyst after reaction

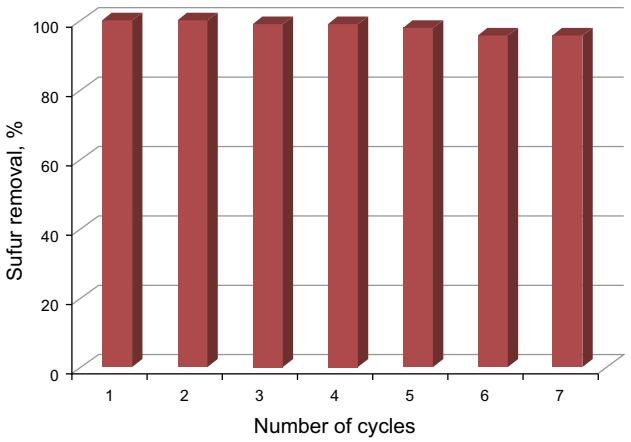

Fig. 10 Recycling performance of hybrid materials. Reaction conditions: mass of catalyst = 0.01 g, T = 60 °C, t = 40 min, molar ratio O/S = 3

noting that the sulfur removal could still reach 93% after cycling for seven cycles. The good recycling ability was ascribed to the stability of silica-supported IL.

4 Conclusion

Silica-supported ionic liquid was successfully prepared by a one-pot hydrothermal method and employed in the heterogeneous oxidative desulfurization of various sulfur compounds. The characterization results indicated that the POM-based IL was uniformly dispersed on the silica matrix and maintained its structural integrity. The sample 0.1$[C_4mim]_3PMo/SiO_2$-250 had excellent catalytic activity for the removal of various sulfur compounds without any solvents and could still reach sulfur removal of 93% after seven cycles. The oxidative efficiency of different substrates decreased in the order of 4,6-DMDBT > 4-MDBT > DBT > BT.

Acknowledgements This work was financially supported by the National Nature Science Foundation of China (Nos. 21776116, 21576122, 21722604), Postdoctoral Foundation of China (No. 2017M621646), Postdoctoral Foundation of Jiangsu Province (No. 2018K083C) and by the Priority Academic Program Development of Jiangsu Higher Education Institutions (PAPD).

References

Akopyan AV, Ivanov EV, Polikarpova PD, Tarakanova AV, Rakhmanov EV, Polyakova OV, et al. Oxidative desulfurization of hydrocarbon fuel with high olefin content. Pet Chem. 2015;55(7):571–4. https://doi.org/10.1134/S0965544115070026.

Dai C, Zhang J, Huang C, Lei Z. Ionic liquids in selective oxidation: catalysts and solvents. Chem Rev. 2017;117(10):6929–83. https://doi.org/10.1021/acs.chemrev.7b00030.

Dong Q, Wang XY, Lu YM, Sun HY, Meng QL, Liu SL, et al. The influence of SiO_2 doping on the microstructure and photochromic behavior of phosphomolybdic acid/polyvinyl pyrrolidone hybrid films. J Mol Struct. 2014;1075:154–8. https://doi.org/10.1016/j.molstruc.2014.07.003.

Ibrahim MH, Hayyan M, Hashim MA, Hayyan A. The role of ionic liquids in desulfurization of fuels: a review. Renew Sustain Energ Rev. 2017;76:1534–49. https://doi.org/10.1016/j.rser.2016.11.194.

Li H, Zhu W, Zhu S, Xia J, Chang Y, Jiang W, et al. The selectivity for sulfur removal from oils: an insight from conceptual density functional theory. AIChE J. 2016;62(6):2087–100. https://doi.org/10.1002/aic.15161.

Li M, Zhang M, Wei A, Zhu W, Xun S, Li Y, et al. Facile synthesis of amphiphilic polyoxometalate-based ionic liquid supported silica induced efficient performance in oxidative desulfurization. J Mol Catal A Chem. 2015;406:23–30. https://doi.org/10.1016/j.molcata.2015.05.007.

Liu F, Kong W, Qi C, Zhu L, Xiao F-S. Design and synthesis of mesoporous polymer-based solid acid catalysts with excellent hydrophobicity and extraordinary catalytic activity. ACS Catal. 2012;2(4):565–72. https://doi.org/10.1021/cs200613p.

Liu L, He C, Li J, Guo J, Yang D, Wei J. Green synthesis of silver nanowires via ultraviolet irradiation catalyzed by phosphomolybdic acid and their antibacterial properties. New J Chem. 2013;37(7):2179–85. https://doi.org/10.1039/c3nj00135k.

Moghadam FR, Azizian S, Bayat M, Yarie M, Kianpour E, Zolfigol MA. Extractive desulfurization of liquid fuel by using a green, neutral and task specific phosphonium ionic liquid with glyceryl moiety: a joint experimental and computational study. Fuel. 2017;208:214–22. https://doi.org/10.1016/j.fuel.2017.07.025.

Paduszyński K, Królikowski M, Zawadzki M, Orzeł P. Computer-aided molecular design of new task-specific ionic liquids for extractive desulfurization of gasoline. ACS Sustainable Chem Eng. 2017;5(10):9032–42. https://doi.org/10.1021/acssuschemeng.7b01932.

Rafiee E, Sahraei S, Moradi GR. Extractive oxidative desulfurization of model oil/crude oil using KSF montmorillonite-supported 12-tungstophosphoric acid. Pet Sci. 2016;13(4):760–9. https://doi.org/10.1007/s12182-016-0127-0.

Rajkumar T, Rao GR. Synthesis and characterization of hybrid molecular material prepared by ionic liquid and silicotungstic acid. Mater Chem Phys. 2008;112(3):853–7. https://doi.org/10.1016/j.matchemphys.2008.06.046.

Ren X, Liu Z, Dong L, Miao G, Liao N, Li Z, et al. Dynamic catalytic adsorptive desulfurization of real diesel over ultra-stable and low-cost silica gel-supported TiO_2. AIChE J. 2018. https://doi.org/10.1002/aic.16055.

Sainero LMG, Damyanova S, Fierro JLG. Methanol oxidation over ZrO_2–SiO_2 supported phosphomolybdic acid. Appl Catal a-Gen. 2001;208(1–2):63–75.

Soleimani M, Bassi A, Margaritis A. Biodesulfurization of refractory organic sulfur compounds in fossil fuels. Biotechnol Adv. 2007;25(6):570–96. https://doi.org/10.1016/j.biotechadv.2007.07.003.

Xu D, Zhu W, Li H, Zhang J, Zou F, Shi H, et al. Oxidative desulfurization of fuels catalyzed by V_2O_5 in ionic liquids at room temperature. Energy Fuels. 2009;23:5929–33. https://doi.org/10.1021/ef900686q.

Xun S, Zhu W, Chang Y, Li H, Zhang M, Jiang W, et al. Synthesis of supported SiW12O40-based ionic liquid catalyst induced solvent-free oxidative deep-desulfurization of fuels. Chem Eng J. 2016;288:608–17. https://doi.org/10.1016/j.cej.2015.12.005.

Xun S, Zhu W, Zheng D, Zhang L, Liu H, Yin S, et al. Synthesis of metal-based ionic liquid supported catalyst and its application in catalytic oxidative desulfurization of fuels. Fuel. 2014;136:358–65. https://doi.org/10.1016/j.fuel.2014.07.029.

Yang E, Yao C, Liu Y, Zhang C, Jia L, Li D, et al. Bamboo-derived porous biochar for efficient adsorption removal of dibenzothiophene from model fuel. Fuel. 2018;211:121–9. https://doi.org/10.1016/j.fuel.2017.07.099.

Zhang J, Liu X, Sun M, Ma X, Han Y. Direct conversion of cellulose to glycolic acid with a phosphomolybdic acid catalyst in a water medium. ACS Catal. 2012;2(8):1698–702. https://doi.org/10.1021/cs300342k.

Zhang L, Wang J, Sun Y, Jiang B, Yang H. Deep oxidative desulfurization of fuels by superbase-derived Lewis acidic ionic liquids. Chem Eng J. 2017a;328:445–53. https://doi.org/10.1016/j.cej.2017.07.060.

Zhang M, Wei Y, Li R, Zhu W, Li H, Zhang Q, et al. Magnetic POM-based mesoporous silica for fast oxidation of aromatic sulfur compounds. Fuel. 2017b;209:545–51. https://doi.org/10.1016/j.fuel.2017.08.001.

Zhang M, Zhu W, Li H, Xun S, Ding W, Liu J, et al. One-pot synthesis, characterization and desulfurization of functional mesoporous W-MCM-41 from POM-based ionic liquids. Chem Eng J. 2014;243:386–93. https://doi.org/10.1016/j.cej.2013.12.093.

Zhang M, Zhu W, Xun S, Li H, Gu Q, Zhao Z, et al. Deep oxidative desulfurization of dibenzothiophene with POM-based hybrid materials in ionic liquids. Chem Eng J. 2013;220:328–36. https://doi.org/10.1016/j.cej.2012.11.138.

Zhao P, Zhang M, Wu Y, Wang J. Heterogeneous selective oxidation of sulfides with H_2O_2 catalyzed by ionic liquid-based polyoxometalate salts. Ind Eng Chem Res. 2012;51(19):6641–7. https://doi.org/10.1021/ie202232j.

Zhou Y, Qu J. Ionic liquids as lubricant additives: a review. ACS Appl Mater Interfaces. 2017;9(4):3209–22. https://doi.org/10.1021/acsami.6b12489.

Zhu WS, Zhu GP, Li HM, Chao YH, Zhang M, Du DL, et al. Catalytic kinetics of oxidative desulfurization with surfactant-type polyoxometalate-based ionic liquids. Fuel Process Technol. 2013;106:70–6. https://doi.org/10.1016/j.fuproc.2012.07.003.